Superoscillating electron wave functions with subdiffraction spots

Roei Remez,[1,*] Yuval Tsur,[1] Peng-Han Lu,[2] Amir H. Tavabi,[2] Rafal E. Dunin-Borkowski,[2] and Ady Arie[1]

[1]*School of Electrical Engineering, Fleischman Faculty of Engineering, Tel-Aviv University, Tel Aviv, Israel*
[2]*Ernst Ruska-Centre for Microscopy and Spectroscopy with Electrons and Peter Grünberg Institute,*
Forschungszentrum Jülich, Jülich, Germany

Almost one and a half centuries ago, Abbe [Arch. Mikrosk. Anat. **9**, 413 (1873)] and shortly after Lord Rayleigh [Philos. Mag. Ser. 5 **8**, 261 (1879)] showed that, when an optical lens is illuminated by a plane wave, a diffraction-limited spot with radius $0.61\lambda/\sin\alpha$ is obtained, where λ is the wavelength and α is the semiangle of the beam's convergence cone. However, spots with much smaller features can be obtained at the focal plane when the lens is illuminated by an appropriately structured beam. Whereas this concept is known for light beams, here, we show how to realize it for a massive-particle wave function, namely, a free electron. We experimentally demonstrate an electron central spot of radius 106 pm, which is more than two times smaller than the diffraction limit of the experimental setup used. In addition, we demonstrate that this central spot can be structured by adding orbital angular momentum to it. The resulting superoscillating vortex beam has a smaller dark core with respect to a regular vortex beam. This family of electron beams having hot spots with arbitrarily small features and tailored structures could be useful for studying electron-matter interactions with subatomic resolution.

Among the methods that are used in light optics for circumventing the Abbe-Rayleigh [1,2] diffraction limit are near-field microscopy [3], metamaterial-based perfect lenses and superlenses [4], and various other super-resolution schemes, e.g., Refs. [5,6]. However, these methods have yet to be demonstrated with matter (e.g., electron) waves. An interesting proposal for manifesting *arbitrarily* small spots for optical microscopy was made in 1952 by Toraldo di Francia [7]. Following earlier work in the microwave regime [8], he proposed putting a series of concentric rings near the lens pupil, thereby modulating the incoming wave so that the central focal spot could be made smaller than the Abbe-Rayleigh limit, accompanied by a peripheral ring of light. In a related development and following concepts that were developed for weak measurements in quantum systems [9], Berry introduced the concept of superoscillating functions and predicted their potential applications for super-resolution microscopy [10]. These superoscillating functions are band-limited functions that locally oscillate faster than their highest Fourier component [9,10]. They have been applied successfully to several applications such as optical microscopy [11], optical beam shaping [12], nonlinear frequency conversion [13], and surface plasmon polariton spot generation [14]. Superoscillations have also been studied in the time domain for applications such as time-dependent subdiffraction focusing [15] and "supertransmission" through absorbing media [16]. The concept of superoscillating waves was not applied until now to matter waves, but it can offer attractive opportunities owing to the much shorter wavelengths of these waves with respect to optical waves. In this Rapid Communication, we concentrate on electron waves and address the following questions: How can we generate a superoscillating wave function? What is the size that can be reached with comparison to the diffraction-limited spot size? Can we obtain hot spots

that are comparable with the size of an atom? What are the limitations on the minimum feature size? And finally, can we structure these superoscillating beams, for example, by adding orbital angular momentum to them, thereby generating superoscillating vortex beams?

Since the beginning of the present decade, the use of holographic masks in electron microscopy has attracted increasing attention, as it allows complete control over the electron amplitude and phase distributions, thus realizing special electron beams [17–19], and opening new possibilities for structured illumination electron microscopy [20,21]. Here, we apply such a mask to form a superoscillatory electron wave function, and discuss its prospects. This wave function, which is designed following a simple analytic derivation [22], features a central spot that can theoretically be made arbitrarily small and routinely smaller than the Abbe-Rayleigh diffraction limit. We note that electron microscopy provides a significantly smaller spot size with respect to optical microscopy, since the de Broglie wavelength of the electron we use is only 2 pm (300 keV), more than five orders of magnitude smaller than the wavelength of visible light; the electron superoscillating hot spot is therefore also much smaller than superoscillations demonstrated so far in light optics. Moreover, unlike photons, charged particles interact with magnetic fields, giving superoscillatory vortex probes interesting prospects for observing and interacting with magnetic materials [17,23].

We now derive a holographic mask design for producing a superoscillatory spot. Unlike a conventional probe-forming lens, which utilizes a uniform, circular hard aperture of diameter D, our proposed superoscillatory probe utilizes a transparency-phase mask $\psi_{\text{mask}}(r)$, where r is the radial distance from the column axis. We use a function previously used in light optics [22,24],

$$\psi_{\text{mask}}(r) \propto \begin{cases} e^{i\pi}, & r \leqslant r_\pi, \\ 1, & r_\pi < r \leqslant r_{\text{max}}, \end{cases} \quad (1)$$

where $0 < r_\pi < r_{\text{max}}$ and $r_{\text{max}} = D/2$. The transmitted wave, i.e., $\psi_{\text{mask}}(r)$, is then condensed by a lens to form the probe

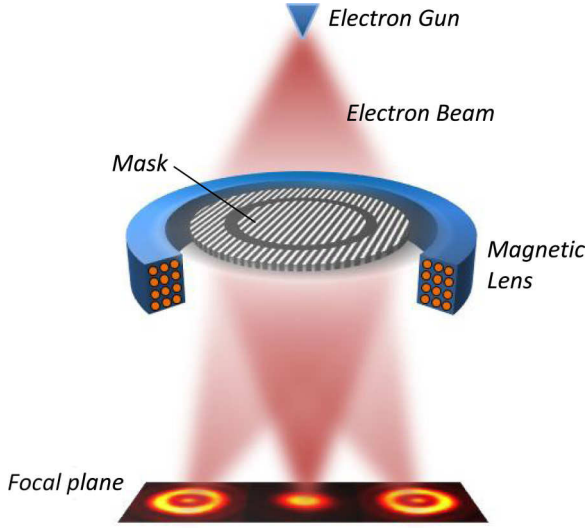*Corresponding author: roei.remez@gmail.com

FIG. 1. Schematic description of superoscillating electron wave-function generation. The desired wave function is created in the +1 and −1 diffraction orders.

wave function, which is proportional to the Fourier transform of $\psi_{\mathrm{mask}}(r)$, [17,25], where the angular coordinate θ is replaced (under the small-angle approximation) by $\theta = r/(f\lambda)$,

$$\psi_{\mathrm{probe}}(a) \propto a^{-1}[r_{\max}J_1(r_{\max}a) - 2r_\pi J_1(r_\pi a)], \qquad (2)$$

where $a = 2\pi r/f\lambda$ and f is the condenser lens focal length. The probability density for electron detection at a normalized distance a from the axis is given by $|\Psi(a)|^2$.

We have implemented this probe-forming mask as an off-axis computer-generated hologram [26]. Among the advantages of this method are the realization of both the phase and the amplitude of the wave function by a binary pass-block mask. The off-axis carrier wave number, $k_c = 2\pi/500$ nm throughout this work, determines the spatial separation between the unwanted zero order and the target superoscillatory first order, in the following computer-generated hologram expression,

$$\psi_{\mathrm{holo}}(r,y) \propto \begin{cases} \mathrm{sgn}[\cos{(k_c y + \pi)}] + 1, & r \leqslant r_\pi, \\ \mathrm{sgn}[\cos{(k_c y)}] + 1, & r_\pi < r \leqslant r_{\max}. \end{cases}$$
$$(3)$$

As illustrated in Fig. 1, the electron wave function will be the Fourier transform of $\psi_{\mathrm{holo}}(r,y)$, for which orders +1 and −1 have the form of Eq. (2),

$$\Psi^{\pm}_{\mathrm{probe}}(a_{\pm}) \propto a_{\pm}^{-1}[r_{\max}J_1(a_{\pm}r_{\max}) - 2r_\pi J_1(a_{\pm}r_\pi)], \qquad (4)$$

where $\vec{r} = (x,y)$, x,y are the Fourier plane coordinates, $\vec{r}_0 = (0, k_c f/k)$, and $a_{\pm} \equiv k|\vec{r} \pm \vec{r}_0|/f$.

We note that it is also possible to realize the desired pattern on the column axis ($r = 0$) using a variable thickness phase mask [21]. In addition, although the outer ring of the superoscillatory spot resembles a vortex beam [27], there is no helical phase present, as evident from Eq. (2), which shows that the probe is purely real. Figures 2(f) and 2(l) present experimentally realized superoscillatory electron probes, which
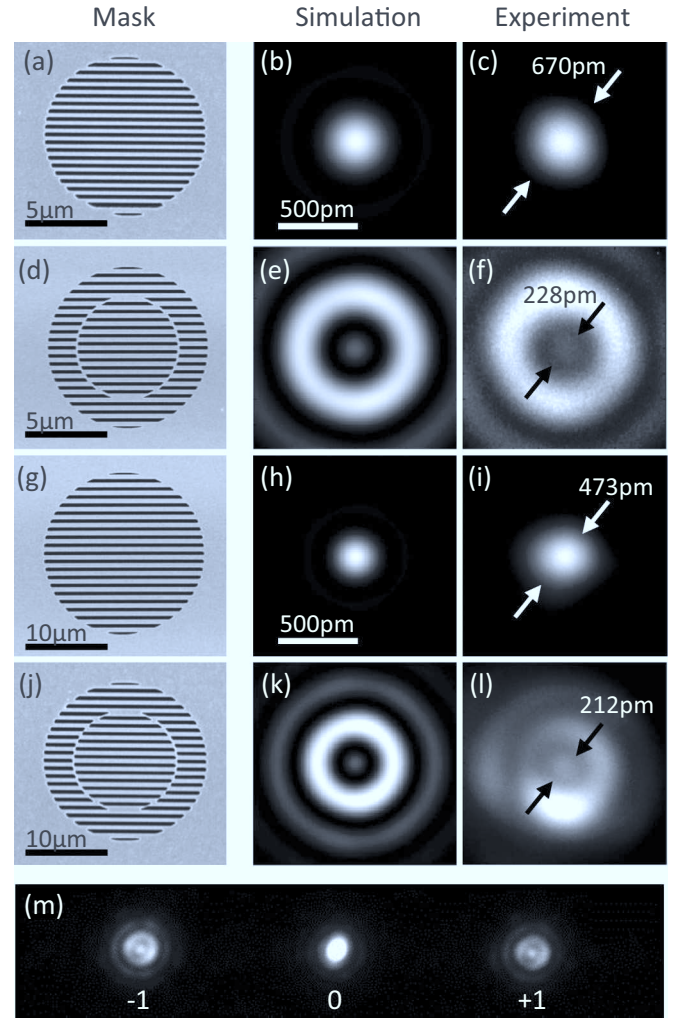

FIG. 2. Scanning electron micrographs of binary amplitude masks [(a), (d), (g), (j)], shown alongside simulations [(b), (e), (h), (k)] and experimental results [(c), (f), (i), (l)] for a circular aperture and superoscillation masks of diameter 10 μm for $\alpha = 3.7$ mrad (rows 1 and 2), and for diameter 20 μm and $\alpha = 5.2$ mrad (rows 3 and 4). The measurements of superoscillating electron beams (f) and (l) exhibit central hot spots of radius 114 and 106 pm, respectively, compared to diffraction-limit's Airy disk radii of 334 and 235 pm, respectively. (m) Three central orders of the diffraction pattern of the mask in (d).

have central hot-spot radii of 114 and 106 pm, i.e., 66% and 55% smaller than the diffraction-limit's Airy radii of 334 and 235 pm for the convergence semiangles used, $\alpha = 3.7$ and 5.2 mrad, respectively. Note that this hot spot is three orders of magnitude smaller with respect to those that were obtained in light optics [11] and is comparable to the size of small atoms [28,29]. The experimental details can be found in Sec. 2 of the Supplemental Material [30]. Looking forward, we postulate that any scattering by the hologram material could be eliminated, along with the use of an amplitude mask, by generating the phase plate [Eq. (1)] via an aberration corrector, in a similar fashion to Airy beam generation [31].

Our experiment was limited by the imaging objective lens of the confocal setup, whose spherical aberration could not be corrected. The spherical aberration of this uncorrected lens
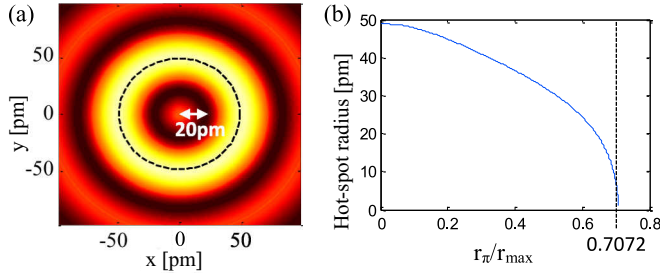
FIG. 3. (a) Simulation of a superoscillating electron beam for an aberration-corrected microscope in both the probe and the imaging parts with $\alpha = 25$ mrad and $r_\pi / r_{max} = 0.64$. The radius of the central hot spot, 20 pm, is only ten times the electron wavelength. The dashed black line marks the diffraction-limited Airy disk. (b) Central lobe radius plotted as a function of r_π / r_{max}. Theoretically, an arbitrarily small electron hot spot can be achieved, as long as factors such as spatial coherence and signal-to-noise ratio are addressed.

explains why, for the larger convergence angle experiment [Figs. 2(g)–2(l)], the circular aperture spot was significantly larger than the theoretical diffraction-limited spot [comparing Fig. 2(i) with Fig. 2(h)]. In Sec. 1 of the Supplemental Material [30], we report a similar experiment for a much smaller convergence angle, hence with negligible spherical and chromatic aberrations, as well as a negligible effect of partial spatial coherence and inelastic scattering. In that case, the experimental spot size is in an excellent agreement with the theoretical prediction, although the smaller convergence angle also leads to a much larger overall spot size.

Let us now consider the fundamental limitations for the hot-spot size. In Fig. 3, we calculate the size of the superoscillating central hot spot in a state-of-the-art microscope, where both the probe-forming and the imaging parts are aberration corrected for a convergence semiangle of 25 mrad, which is slightly more conservative than the value of $\alpha = 32.4$ mrad achieved by Sawada *et al.* [32]. In contrast to conventional spots, which are bounded by diffraction associated with the aforementioned Airy disk, a superoscillating spot can be arbitrary small for large enough values of r_π [see Fig. 3(b)]. This conceptually includes hot spots that are smaller than the wavelength, as was already demonstrated in light optics [11]. However, significant limitations stem from the low relative intensity of the hot spot, as we discuss below. In a more practical sense, in the following we consider also incoherent aberrations, namely, partial spatial coherence and chromatic aberration.

Spatial incoherence. The field emission gun tip is demagnified when imaged onto the specimen plane to form a small probe. The size of the image of the gun determines the amount of smear expected for the measured wave function. In a state-of-the art scanning transmission electron microscope (STEM), this smear is about 7 pm [32]. As simulated in Figs. 4(a)–4(d), the 10λ radius hot spot described in Fig. 3(a) can indeed be realized experimentally using today's technology.

We stress that, even when the source is spatially incoherent, the wave front of each emitted electron contains the superoscillation (which can be arbitrarily small). However, the reduction in contrast caused by spatial incoherence would hamper the *observation* of a small superoscillation within a large ensemble of electrons.
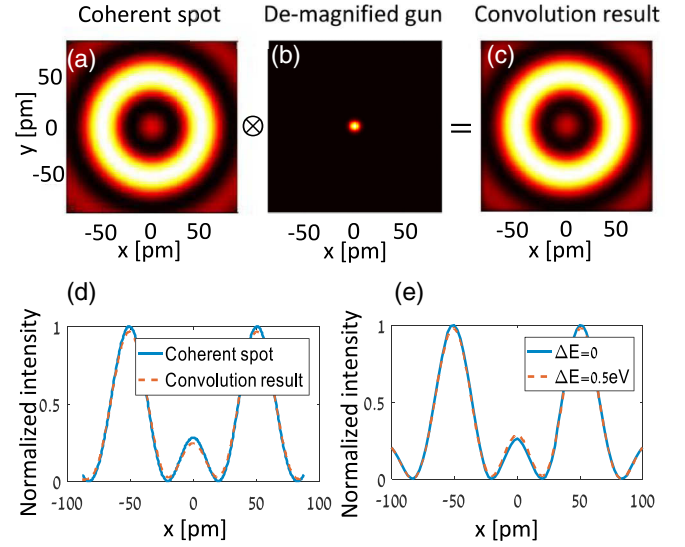

FIG. 4. The effect of spatial and temporal incoherence on a 10λ superoscillating hot spot for $\alpha = 25$ mrad. (a) The superoscillating probe assuming perfect coherence. (b) Gun shape after demagnification, having a full width at half maximum of 7 pm. (c) The convolution of (a) and (b). (d) Cross sections of (a) (solid) and (c) (dashed). (e) The effect of chromatic aberration for $\alpha = 25$ mrad, Cc = 1.35 mm, $E = 300$ keV, for $\Delta E = 0$ eV (solid blue) and $\Delta E = 0.5$ eV (dashed red). Incoherent summation was carried out over an ensemble of electrons having a Gaussian energy distribution with $\sigma_E = \Delta E / \sqrt{8 \ln(2)} = 0.21$ eV.

Temporal incoherence: The energy uncertainty of the electron, attributed to the gun and the high-voltage supply, results in chromatic aberration. We split the discussion into two effects. First, the focal length of the lens changes with the wavelength of the electron, causing different electron wave functions to be slightly defocused compared to the designed wavelength. We performed simulations for a chromatic aberration coefficient Cc of 1.35 mm and an energy spread of $\Delta E = 0.5$ eV, which is determined as a sum of squares of the electron gun energy spread of 0.4 eV [32], a typical instability of the high-voltage supply of 0.2 eV, and a typical instability of the condenser system, equivalent to 0.2 eV. The convergence angle was $\alpha = 25$ mrad. As Fig. 4(e) shows, this chromatic aberration causes a negligible smear of the hot spot. Second, even if Cc is zero, the scale of the probe plane changes by an amount $\Delta \lambda / \lambda$, which is around $10^{-6} \ll 1$ and therefore gives a negligible smearing effect.

We note that temporal incoherence can be reduced by using an electron monochromator [33], which transfers the problem to a signal-to-noise ratio issue (which can be compensated by using a large exposure time, assuming that the electronics and mechanics are stable).

Inelastic scattering. Some of the contrast degradation apparent in Fig. 2 is attributed to inelastic scattering from the parts of the mechanically supporting 100-nm SiN, which were not milled. Removing this support (for example, see the mask in Ref. [17]) would lead to the exclusion of any inelastic scattering, thus enabling a smaller spot.

Overall stability and signal-to-noise ratio. The intensity of the hot-spot in Fig. 3(a) is only three times lower than that of
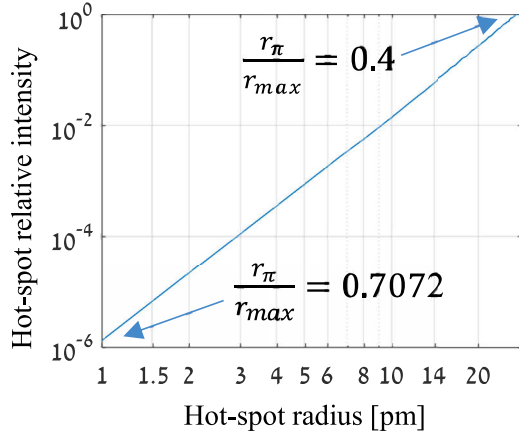
FIG. 5. Hot-spot peak intensity divided by sidelobe peak intensity, shown as a function of hot-spot radius. The calculations were performed for a convergence semiangle of 25 mrad and $\lambda = 2$ pm. Each point in this plot corresponds to a different value of $r_\pi/r_{\max}$.

the peripheral ring. Therefore, Figs. 2 and 3(a) are not different in terms of the signal-to-noise ratio. When trying to decrease the hot-spot size towards the de Broglie wavelength, significant limitations stem from both the low relative intensity of the hot spot, as shown in Fig. 5, and the mechanical stability of the microscope column.

As demonstrated recently by Singh *et al.* [34] in light optics, the central spot of a superoscillating beam can be structured. Here, we implement this concept in electron optics to create superoscillating electron vortex beams. Such vortex beams are characterized by a helical phase and carry orbital angular momentum (OAM). Owing to the on-axis phase singularity, these beams are characterized by a doughnut shape, with a dark central core. The generation of electron vortex beams [17,21,25,27] and their application for studying magnetic dichroism [17,35] and for rotating nanoparticles [36] have generated much interest in recent years. The superoscillating vortex beams as shown here have smaller dark cores compared to conventional vortex beams, thereby potentially enabling one to study the transfer of angular momentum between electrons and matter with improved resolution.

To generate these beams, we used the following mask design,

$$\psi_{\text{holo}}(r,y) \propto \begin{cases} \text{sgn}[\cos(k_c y + l\phi + \pi)] + 1, & r \leqslant r_\pi, \\ \text{sgn}[\cos(k_c y + l\phi)] + 1, & r_\pi < r \leqslant r_{\max}, \end{cases}$$

(5)

where ϕ is the angle with the y axis at the plane of the mask and l is an integer [37]. In comparison to Eq. (1), which was used to generate a nonstructured superoscillating beam, a helical phase term $\exp(il\phi)$ was added. This adds an OAM of $\hbar l$ per electron. In Figs. 6(f) and 6(l), we show experimentally electron beams with OAMs of $1\hbar$ and $3\hbar$, having inner rings that are smaller by 20% and 32%, respectively, compared to conventional beams with the same OAM values. This experiment was performed with $\alpha = 0.05$ mrad and mask diameters of 10 μm, but could easily be repeated for a larger convergence angle similarly to Fig. 2. As shown by Singh *et al.* [34] for the case of light beams,
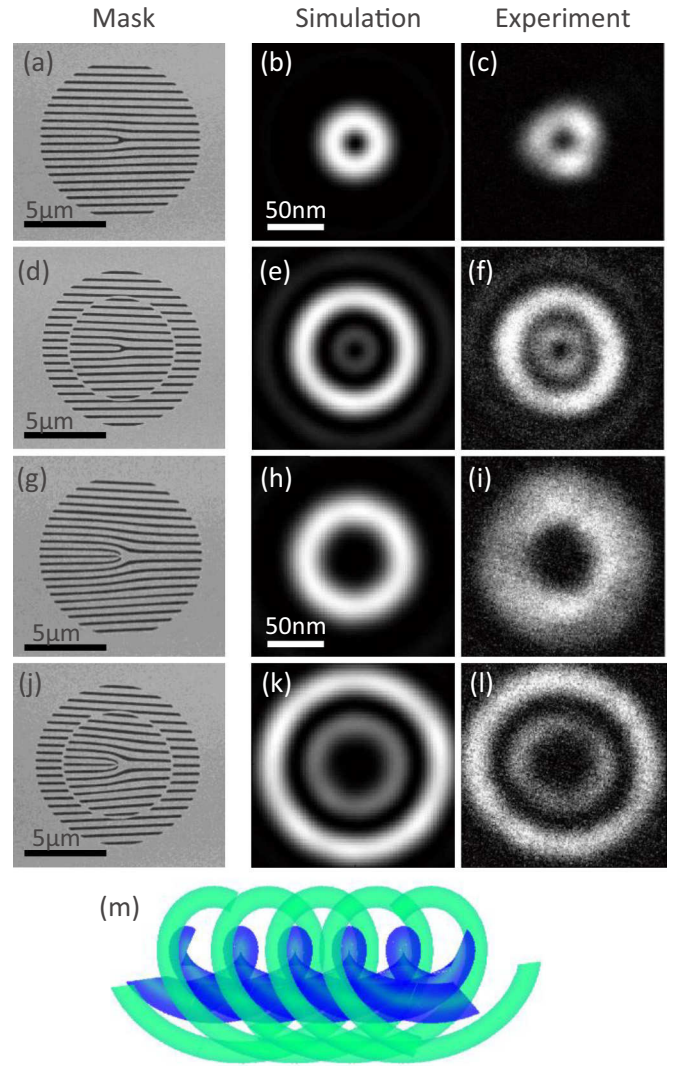
FIG. 6. Superoscillating electron vortex beams. Vortex and superoscillating $r_\pi/r_{\max} = 0.68$ vortex beams with OAM = 1 (rows 1 and 2, respectively) and OAM = 3 (rows 3 and 4). (m) Schematic description of equiphase surfaces of OAM = 3 superoscillatory electron vortex (row 4), with π-phase-shifted inner and outer rings.

other structures with interesting properties can be imposed on a superoscillating hot spot—for example, Airy functions that exhibit self-acceleration, or multilobed Hermite-Gauss functions.

In this Rapid Communication, we have presented superoscillating wave functions for a massive particle, featuring a central spot that is smaller than the Abbe-Rayleigh diffraction limit, as well as superoscillating vortex beams. These can be the first members in a family of shaped superoscillatory electron wave functions. The transmission electron microscope operates fundamentally in the single-particle regime, supporting the assertion that superoscillation stems from interference of the wave function with itself [38]. We have shown a straightforward, highly efficient method to produce the wave function, generated for an arbitrary focal length. We have demonstrated how a hot spot only ten times the electron wavelength can be created nowadays using this method.

In addition, with improving technology, a subwavelength electron hot spot might become possible. We believe that this demonstration opens a wide range of possibilities in electron wave-function manipulation, in order to create dense oscillations that were previously thought impossible in finite electron wave functions, such as subdiffraction needles [39] that can enable increased electron beam lithography resolution, superoscillatory shape-preserving beams [40], and enhanced electron microscope images, as was demonstrated with light [11,41,42]. Arbitrarily dense electron wave functions, having a tailored shape, can be created by our method using prolate spherical wave functions [43] (with a penalty to the average amplitude in the superoscillating area). The superoscillation wave function can also be used as an initial state for the realization of weak measurements of displacement in quantum systems [38,44]. In addition, we note that superoscillations could be created using the concept presented here with other massive particles and even large molecules [45].

[1] E. Abbe, Beiträge zur theorie des mikroskops und der mikroskopischen wahrnehmung, Arch. Mikrosk. Anat. **9**, 413 (1873).

[2] F. R. S. Rayleigh, XXXI. Investigations in optics, with special reference to the spectroscope, Philos. Mag. Ser. 5 **8**, 261 (1879).

[3] U. Dürig, D. W. Pohl, and F. Rohner, Near-field optical-scanning microscopy, J. Appl. Phys. **59**, 3318 (1986).

[4] J. B. Pendry, Negative Refraction Makes a Perfect Lens, Phys. Rev. Lett. **85**, 3966 (2000).

[5] S. W. Hell, Microscopy and its focal switch, Nat. Methods **6**, 24 (2009).

[6] W. Lukosz, Optical systems with resolving powers exceeding the classical limit, J. Opt. Soc. Am. **56**, 1463 (1966).

[7] G. Toraldo di Francia, Super-gain antennas and optical resolving power, Nuovo Cimento **9**, 426 (1952).

[8] S. A. Schelkunoff, A mathematical theory of linear arrays, Bell Syst. Tech. J. **22**, 80 (1943).

[9] Y. Aharonov, D. Z. Albert, and L. Vaidman, How the Result of a Measurement of a Component of the Spin of a Spin-1/2 Particle can Turn Out to be 100, Phys. Rev. Lett. **60**, 1351 (1988).

[10] M. Berry, Faster than Fourier, in *Quantum Coherence and Reality: In Celebration of the 60th Birthday of Yakir Aharonov*, edited by J. S. Anandan and J. L. Safko (World Scientific, Singapore, 1994), pp. 55–65.

[11] E. T. F. Rogers, J. Lindberg, T. Roy, S. Savo, J. E. Chad, M. R. Dennis, and N. I. Zheludev, A super-oscillatory lens optical microscope for subwavelength imaging, Nat. Mater. **11**, 432 (2012).

[12] E. Greenfield, R. Schley, I. Hurwitz, J. Nemirovsky, K. G. Makris, and M. Segev, Experimental generation of arbitrarily shaped diffractionless superoscillatory optical beams, Opt. Express **21**, 13425 (2013).

[13] R. Remez and A. Arie, Super-narrow frequency conversion, Optica **2**, 472 (2015).

[14] G. Yuan, E. T. F. Rogers, T. Roy, L. Du, Z. Shen, and N. I. Zheludev, Plasmonic super-oscillations and sub-diffraction focusing, in *CLEO: QELS_Fundamental Science* (Optical Society of America, Washington, DC, 2014).

[15] M. Dubois, E. Bossy, S. Enoch, S. Guenneau, G. Lerosey, and P. Sebbah, Time-Driven Superoscillations with Negative Refraction, Phys. Rev. Lett. **114**, 013902 (2015).

[16] Y. Eliezer and A. Bahabad, Super-transmission: The delivery of superoscillations through the absorbing resonance of a dielectric medium, Opt. Express **22**, 31212 (2014).

[17] J. Verbeeck, H. Tian, and P. Schattschneider, Production and application of electron vortex beams, Nature (London) **467**, 301 (2010).

[18] N. Voloch-Bloch, Y. Lereah, Y. Lilach, A. Gover, and A. Arie, Generation of electron Airy beams, Nature (London) **494**, 331 (2013).

[19] V. Grillo, G. Carlo Gazzadi, E. Karimi, E. Mafakheri, R. W. Boyd, and S. Frabboni, Highly efficient electron vortex beams generated by nanofabricated phase holograms, Appl. Phys. Lett. **104**, 43109 (2014).

[20] C. Ophus, J. Ciston, J. Pierce, T. R. Harvey, J. Chess, B. J. McMorran, C. Czarnik, H. H. Rose, and P. Ercius, Efficient linear phase contrast in scanning transmission electron microscopy with matched illumination and detector interferometry, Nat. Commun. **7**, 10719 (2016).

[21] R. Shiloh, Y. Lereah, Y. Lilach, and A. Arie, Sculpturing the electron wave function using nanoscale phase masks, Ultramicroscopy **144**, 26 (2014).

[22] M. P. Cagigal, J. E. Oti, V. F. Canales, and P. J. Valle, Analytical design of superresolving phase filters, Opt. Commun. **241**, 249 (2004).

[23] K. Y. Bliokh, Y. P. Bliokh, S. Savel'ev, and F. Nori, Semiclassical Dynamics of Electron Wave Packet States with Phase Vortices, Phys. Rev. Lett. **99**, 190404 (2007).

[24] Z. S. Hegedus and V. Sarafis, Superresolving filters in confocally scanned imaging systems, J. Opt. Soc. Am. A **3**, 1892 (1986).

[25] B. J. McMorran, A. Agrawal, I. M. Anderson, A. A. Herzing, H. J. Lezec, J. J. McClelland, and J. Unguris, Electron vortex beams with high quanta of orbital angular momentum, Science **331**, 192 (2011).

[26] W. H. Lee, Binary computer-generated holograms, Appl. Opt. **18**, 3661 (1979).

[27] M. Uchida and A. Tonomura, Generation of electron beams carrying orbital angular momentum, Nature (London) **464**, 737 (2010).

[28] R. E. Dunin-Borkowski and J. M. Cowley, Simulations for imaging with atomic focusers, Acta Crystallogr., Sect. A: Found. Crystallogr. **55**, 119 (1999).

[29] J. M. Cowley, J. C. H. Spence, and V. V. Smirnov, The enhancement of electron microscope resolution by use of atomic focusers, Ultramicroscopy **68**, 135 (1997).

[30] See Supplemental Material at http://link.aps.org/supplemental/10.1103/PhysRevA.95.031802 for the low convergence angle experiment, experimental details, and the mathematical criterion for superoscillations.

[31] G. Guzzinati, L. Clark, A. Béché, R. Juchtmans, R. Van Boxem, M. Mazilu, and J. Verbeeck, Prospects for versatile phase manipulation in the TEM: Beyond aberration correction, Ultramicroscopy **151**, 85 (2015).

[32] H. Sawada, N. Shimura, F. Hosokawa, N. Shibata, and Y. Ikuhara, Resolving 45-pm-separated Si-Si atomic columns with an aberration-corrected STEM, Microscopy **64**, 213 (2015).

[33] P. C. Tiemeijer, M. Bischoff, B. Freitag, and C. Kisielowski, Using a monochromator to improve the resolution in TEM to below 0.5 Å. Part I: Creating highly coherent monochromated illumination, Ultramicroscopy **114**, 72 (2012).

[34] B. K. Singh, H. Nagar, Y. Roichman, and A. Arie, Particle manipulation beyond the diffraction limit using structured super-oscillating light beams, Light Sci. Appl. (to be published) (2017).

[35] S. Lloyd, M. Babiker, and J. Yuan, Quantized Orbital Angular Momentum Transfer and Magnetic Dichroism in the Interaction of Electron Vortices with Matter, Phys. Rev. Lett. **108**, 074802 (2012).

[36] J. Verbeeck, H. Tian, and G. Van Tendeloo, How to manipulate nanoparticles with an electron beam? Adv. Mater. **25**, 1114 (2013).

[37] Recently, we became aware of a work showing higher-order vortex beams which resemble our results. However, our method allows an arbitrarily small inner ring by controlling r_π. See G. Thirunavukkarasu *et al.*, Normal modes and mode transformation of pure electron vortex beams, Philos. Trans. R. Soc., A **375**, 20150438 (2017).

[38] G. Yuan, S. Vezzoli, C. Altuzarra, E. T. F. Rogers, C. Couteau, C. Soci, and N. I. Zheludev, Quantum super-oscillation of a single photon, Light: Sci. Appl. **5**, e16127, (2016).

[39] G. Yuan, E. T. F. Rogers, T. Roy, G. Adamo, Z. Shen, and N. I. Zheludev, Planar super-oscillatory lens for sub-diffraction optical needles at violet wavelengths, Sci. Rep. **4**, 6333 (2014).

[40] K. G. Makris and D. Psaltis, Superoscillatory diffraction-free beams, Opt. Lett. **36**, 4335 (2011).

[41] A. M. H. Wong and G. V Eleftheriades, An optical super-microscope for far-field, real-time imaging beyond the diffraction limit, Sci. Rep. **3**, 1715 (2013).

[42] E. T. F. Rogers and N. I. Zheludev, Optical super-oscillations: sub-wavelength light focusing and super-resolution imaging, J. Opt. **15**, 94008 (2013).

[43] D. Slepian and H. Pollak, Prolate spheroidal wave functions, Fourier analysis and uncertainty—I, Bell Syst. Tech. J. **40**, 43 (1961).

[44] P. Ben Dixon, D. J. Starling, A. N. Jordan, and J. C. Howell, Ultrasensitive Beam Deflection Measurement via Interferometric Weak Value Amplification, Phys. Rev. Lett. **102**, 173601 (2009).

[45] T. Juffmann, A. Milic, M. Müllneritsch, P. Asenbaum, A. Tsukernik, J. Tüxen, M. Mayor, O. Cheshnovsky, and M. Arndt, Real-time single-molecule imaging of quantum interference, Nat. Nanotechnol. **7**, 297 (2012).